ACS APPLIED MATERIALS & INTERFACES

RESEARCH ARTICLE

www.acsami.org

Silver-Coated Dye-Embedded Silica Beads: A Core Material of Dual Tagging Sensors Based on Fluorescence and Raman Scattering

Kwan Kim,*[,†] Hyang Bong Lee,[†] Jeong-Yong Choi,[†] and Kuan Soo Shin*[,‡]

[†]Department of Chemistry, Seoul National University, Seoul 151-742, Korea and

[‡]Department of Chemistry, Soongsil University, Seoul 156-743, Korea

ABSTRACT: We have developed a new type of dual-tag sensor for immunoassays, operating via both fluorescence and surface-enhanced Raman scattering (SERS). A one-shot fluorescence image over the whole specimen allows us to save considerable time because any unnecessary time-consuming SERS measurements can be avoided from the signature of the fluorescence. Dye-embedded silica beads are prepared initially, and then SERS-active silver is coated onto them via a very simple electroless-plating method. The Raman markers are subsequently assembled onto the Ag-coated silica beads, after which they are stabilized by silanization via a biomimetic process in which a poly(allylamine hydrochloride) layer formed on the Raman markers by a layer-by-layer deposition method acting as a scaffold for guiding silicification. In the final stage, specific antibodies are attached to the silica surface in order to detect target antigens. The fluorescence signal of the embedded dye can be used as a fast readout system of molecular recognition, whereas the SERS signals are subsequently used as the signature of specific molecular interactions. In this way, the antibody-grafted particles were found to recognize antigens down to 1×10^{-10} g mL^{-1} solely by the SERS peaks of the Raman markers.

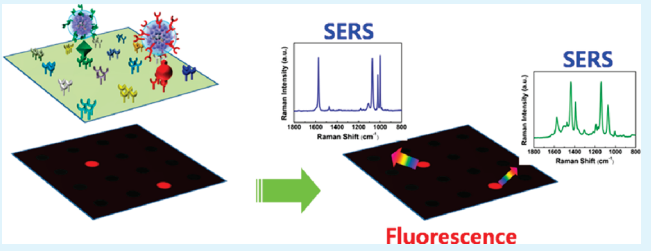

KEYWORDS: silica bead, silver nanostructure, rhodamine B isothiocyanate, surface-enhanced Raman scattering, fluorescence, antigen−antibody binding

1. INTRODUCTION

Immunoassays based on antigen−antibody binding are a powerful analytical tool for biochemical studies, clinical diagnostics, and environmental monitoring.[1−4] Many different immunoassay readout techniques such as scintillation counting, fluorescence, chemiluminescence, electrochemical and enzymatic methods, and Raman scattering have been exploited for the detection of the antigen−antibody binding.[5−17] Among these techniques, fluorescence is currently the principal detection method in bioassays because high sensitivity is critical for immunoassay detection. It has, however, inherent drawbacks, such as photobleaching, narrow excitation with broad emission profiles, and peak overlapping in multiplexed experiments.

Raman scattering is a well-established vibrational spectroscopic method used in chemical analysis. However, its signals are generally too weak to be used for immunoassay because most molecules exhibit low Raman scattering cross-sections. Surface-enhanced Raman scattering (SERS) offers a chance to increase the Raman intensities of molecules adsorbed onto nanostructured Au or Ag surfaces by about 6−14 orders of magnitude, even allowing the detection of the signal of a single molecule.[18−21] In addition, SERS is insensitive to humidity, oxygen and other quenchers, and thus a promising method for sensitive biological identifications and detections.[11,13,22]

As described above, fluorescence can hardly be adopted in the multiplex experiments. We believe that fluorescence can nonetheless be used fruitfully even in multiplex experiments when it is coupled with SERS. This is particularly because the conventional fluorescence microscope image of a large area of the specimen can be captured in one shot, although the SERS measurement is usually time-consuming due to the necessity of through focus scan with certain step and Raman acquisition at each step. Only a single fluorescence reading over the whole specimen would be just enough to confirm the occurrence of any antigen−antibody interactions whose details could be revealed later by SERS. Then, any unnecessary SERS measurements can be avoided from the signature of the fluorescence. This concept is illustrated in Scheme 1b.

Hundreds of different Raman tags can readily be incorporated into a SERS-active nanostructure. Several groups have indeed developed various types of multimodal tags based on fluorescence and SERS that can be used in diagnostic bioassays.[23−25] Cho and coworker have developed multifunctional fluorescent SERS tagging materials (F-SERS dots) composed of Ag nanoparticle-embedded silica spheres with organic dye and Raman labels for multiplex targeting, tracking, and imaging of biological events.[23,24] Pallaoro et al. recently reported that small Ag clusters incorporating both the pH-sensitive probe molecule and a fluorescent dye could be used to determine the local pH from spatially mapped SERS spectra correlated with the fluorescence.[25] We have also recently demonstrated that SERS-active substrates can be fabricated to possess

Received: October 2, 2010
Accepted: December 13, 2010
Published: December 29, 2010

Scheme 1. (a) Illustration of Fabrication Processes of RhBITC-Embedded SiO_2@Ag Beads Modified Further with Antibodies for Multiplex Immunoassays; (b) Illustration of Basic Concept of Dual-Tagging Sensor[a]

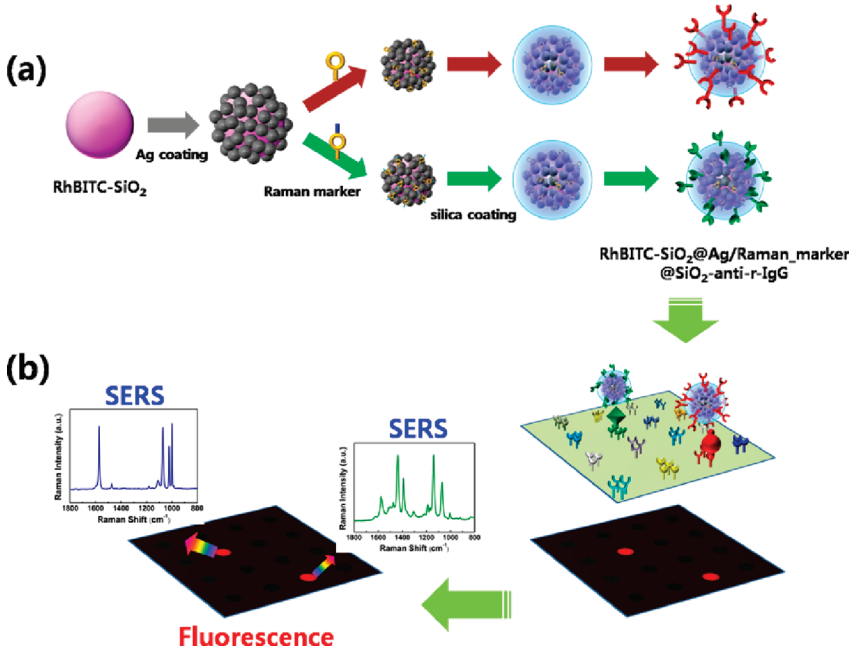

[a] A 2D array consisting of hundreds of antibodies is allowed first to interact with an analyte solution containing antigens that can bind to the antibodies, and then soaked in a solution containing diverse SERS active particles that are derivatized with proper antibodies, but possessing respective Raman markers along with a common fluorescent dye. The interacted areas are identified immediately from the fluorescence image, and then subject to Raman spectral analyses to identify specific interactions.

fluorescence by coating them with fluorescent-grafted polyelectrolytes.[26,27] The Raman markers were assembled initially onto the Ag-coated silica beads (SiO_2@Ag),[26,27] after which they were stabilized by a layer-by-layer (LbL) deposition of anionic and cationic polyelectrolytes including a dye-grafted polyelectrolyte.[28] In the final stage, the dual tagging sensors were assembled onto them with specific antibodies (antihuman-IgG or antirabbit-IgG) to detect target antigens (human-IgG or rabbit-IgG). The fluorescence signal was used as a fast readout system of molecular recognition, while the SERS signals were used subsequently as the signature of specific molecular interactions: The antibody-grafted SiO_2@Ag particles were able to recognize antigens down to 1×10^{-10} g mL^{-1} solely by the SERS peaks of Raman markers.

In this work, two modifications are made to improve the ease of use and the stability of our dual-tag sensor. First, dye molecules are embedded into silica beads that subsequently serve as the platform to develop SERS-active Ag nanoaggregates. Second, Raman marker-adsorbed Ag nanoaggregates are coated with a silica shell to secure the stability of the SERS activity. We demonstrate that the outermost silica shell can easily be derivatized with antibodies to detect specific target antigens. The strategy to assemble dye-embedded dual-tag sensors is illustrated in Scheme 1a. As surmised, the fluorescence signal is used first as an indicator of molecular recognition, and the SERS signals are used subsequently to gain identification of the specific molecular interactions.

2. EXPERIMENTAL PROCEDURES

Chemicals. Rhodamine B isothiocyanate (RhBITC, 97%), n-hexanol (99%), cyclohexane (99%), tetraethyl orthosilicate (TEOS, 99%), (3-aminopropyl)triethoxysilane (APTS, 99%), silver nitrate ($AgNO_3$, 99%), Ag powder (μAg, 99.9+%) with a particle size of 2.0 μm, butylamine (99%), benzenethiol (BT, 99+%), 4-aminobenznethiol (4ABT, 97%), poly(allylamine hydrochloride) (PAH, MW∼70 kDa), poly(acrylic acid) (PAA, MW∼100 kDa), Triton X-100 (TX-100), human-IgG (h-IgG), rabbit-IgG (r-IgG), goat antihuman-IgG (anti-h-IgG), mouse antirabbit-IgG (anti-r-IgG), glutaraldehyde (GA), and bovine serum albumin (BSA) were purchased from Aldrich and used as received. Other chemicals, unless specified, were of reagent grade. Highly pure water (Millipore Milli-Q system), of resistivity greater than 18.0 MΩ cm, was used throughout.

Preparation of Dye-Embedded SiO_2 Beads. Dye-Embedded silica beads were synthesized using a water-in-oil (W/O) microemulsion method.[29,30] RhBITC (3 mg) was reacted with 100 μL of APTS in 500 μL of ethanol overnight in the dark. The W/O micoemulsion was prepared by mixing 5 mL of TX-100, 15 mL of cyclohexane, 5 mL of hexanol, 500 μL of RhBITC-modified dye solution, 2 mL of water, and 400 μL of TEOS. Subsequently, ammonia ethanol solution (0.1 mL, 30%) was added dropwise under vigorous stirring and left overnight while stirring to become a turbid solution. The mixture was centrifuged to remove the suspension, and the residual was washed thoroughly with ethanol.

Ag Deposition on Dye-Embedded SiO_2 Beads. To deposit silver onto the dye-embedded silica beads, the cleaned RhBITC-embedded SiO_2 beads in ethanol was added into the silvering medium to a final concentration of 0.10 mg mL^{-1} (w/v, dried bead mass/ethanol) and then incubated for 50 min at 50 °C with vigorous shaking. As a silvering mixture, the concentrations of $AgNO_3$ and butylamine were each maintained at 1 mM.[31] After rinsing with ethanol, the RhBITC-embedded SiO_2@Ag beads were redispersed in ethanol under sonication for 5 min.

Assembly of Raman Markers on Modified SiO_2 Beads. In order to use the RhBITC-embedded SiO_2@Ag beads as a core material for molecular sensors operating via both SERS and fluorescence, first, 4ABT (or BT) molecule as a Raman marker was assembled onto the surface of RhBITC-embedded SiO_2@Ag beads. Specifically, 0.1 mg of RhBITC-embedded SiO_2@Ag beads was placed in a vial into which

10 mL of 1 mM ethanolic 4ABT (or BT) solution was subsequently added. After 3 h, the resulting solution was centrifuged and then rinsed with ethanol to remove the excess Raman markers.

Silanization of Assembled SiO_2 Beads. The silanization was performed after three bilayers of PAA and PAH were deposited onto the Raman marker molecules for guiding silanization. The initial deposition of polyelectrolytes was accomplished by dipping the Raman marker-adsorbed, dye-embedded SiO_2@Ag beads sequentially into the PAA and PAH solutions (2 mg mL^{-1}) for 10 min at room temperature. Subsequently, 0.05 g of the beads was weighed and then poured, under sonication, into a mixture composed of 4 mL of water and 25 mL of 2-propanol. To this mixture were added ammonia and TEOS, to a final concentration of 0.15 and 0.1 M, respectively, and the whole mixture was then left to react for 2 h at room temperature. The reacted particles were collected after centrifugation, and rinsed with water and ethanol.

Immobilization of Antibodies on SiO_2 Beads to Detect Antigens. To immobilize any antibodies on the silica shells, we first allowed the silica-coated beads to react with APTS (in 0.1 mM ethanolic solution) in order to have amine functionality. The beads were subsequently shaken for 1 h in a 2.5% aqueous solution of GA, followed by washing with water and centrifugation.[32−34] The resulting beads were incubated for 1 h in a PBS buffer containing 100 μg mL^{-1} anti-h-IgG (or anti-r-IgG) with shaking. After they were rinsed with PBS, these antibody-modified beads were redispersed in 2 mM Tris-HCl buffer solution containing 1% BSA (pH 7.2) and stored at 4 °C while not in use. For an immunoassay, two bilayers of PAA and PAH were separately assembled on a cleaned glass slide. Thereafter, the slide was successively incubated in a GA solution (2.5%) for 3 h, in a solution of anti-h-IgG (or anti-r-IgG) (100 μg mL^{-1}) for 12 h at 4 °C and then in a BSA (100 μg mL^{-1}) solution for 3 h. The antibody-modified slide was subsequently incubated for 30 min in a PBS buffer (pH 7.2) containing 1% BSA and different amounts of h-IgG antigen (or r-IgG antigen). The antigen-adsorbed substrate was thereafter immersed in a solution containing anti-h-IgG (or anti-r-IgG) modified Ag-coated silica beads for 3 h under gentle shaking. After washing with pure water, the modified glass slide was subjected to confocal laser scanning microscopy and Raman spectroscopy measurements.

Instrumentation. UV/vis absorption spectra were obtained using a SCINCO S-4100 spectrometer. Photoluminescence (PL) measurements were carried out on a JASCO FP-750 with an excitation wavelength of 514.5 nm. The zeta potential of silica beads was measured in water by using electrophoretic light scattering spectrophotometer (ELS-8000, OTSUKA Electronics Co. Ltd., Japan). X-ray diffraction (XRD) patterns were obtained on a Bruker D5005 powder diffractometer for a 2θ range of 30° to 80° at an angular resolution of 0.05° using Cu Kα (1.5406 Å) radiation. Confocal laser scanning microscopy (CLSM) images were captured with a Carl Zeiss-LSM510 equipped with a 543 nm line of a He/Ne laser and a water immersion objective. Field emission scanning electron microscopy (FE-SEM) images were obtained with a JSM-6700F field emission scanning electron microscope. Transmission electron microscopy (TEM) images were obtained on a JEM-200CX transmission electron microscope. The Raman spectral measurements were conducted using a Renishaw Raman system model 2000 spectrometer equipped with an integral microscope (Olympus BH2-UMA). The 514.5 nm radiation from a 20 mW air-cooled Ar^+ laser (Melles-Griot Model 351MA520) and the 632.8 nm radiation from a 17 mW air-cooled He/Ne laser (Spectra Physics model 127) were used as the excitation sources. Raman scattering was detected in backscattering geometry (180°) using a Peltier cooled (−70 °C) charge-coupled device (CCD) camera (400 × 600 pixels). The Raman band of a silicon wafer at 520 cm^{-1} was used to calibrate the spectrometer.

3. RESULTS AND DISCUSSION

Characterization of Dye-Embedded SiO_2 Beads. According to the FE-SEM image shown in Figure 1a, the RhBITC-embedded silica beads prepared in this work are spherical with a mean diameter of 95 ± 11 nm; the inset is a photograph of the RhBITC-embedded silica beads solution. The dried silica beads exhibited a very broad O−H stretching band in the region of 3200 - 3600 cm^{-1} in the IR spectrum.[35] A zeta potential measurement indicates that the silica beads are negatively charged in absolute ethanol, i.e. −37.8 ± 9.7 mV, suggesting that the surface hydroxyl groups are deprotonated in absolute ethanol. Because of these negative charges, silver ions readily approached the silica beads for the growth of Ag nanoparticles.

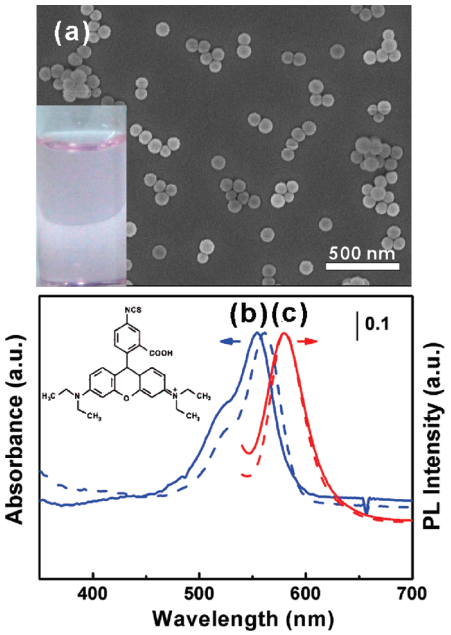

Figure 1. (a) FE-SEM image of RhBITC-embedded silica beads synthesized in this work. The inset is a photograph of the beads solution. (b) UV/vis extinction spectrum of RhBITC in ethanol (blue solid line) and that of RhBITC-embedded silica beads in ethanol (blue dashed line). (c) PL spectrum of RhBITC in ethanol (red solid line) and that of RhBITC-embedded silica beads in ethanol (red dashed line).

In Figure 1b, the blue solid line represents the UV/vis spectrum of RhBITC in ethanol, while the blue dashed line shows the corresponding spectrum taken for RhBITC-embedded silica beads in ethanol: The molecular structure of RhBITC is shown in the inset. The two spectra are almost the same; a slight difference in the peak position, one at 520 nm and the other at 555 nm, is due to the environment and/or the relatively close arrangement of RhBITC on the inside of the beads (vide infra). The RhBITC concentration in the silica beads was estimated by the difference of emission intensity in solution before and after the bead formation, and the number of RhBITC molecules embedded in each bead was then computed to be ∼20000. As shown in Figure 1c, the RhBITC-embedded silica beads also displayed an emission spectrum with its maximal wavelength at 578 nm upon excitation at 514 nm. In Figure 1c, the red dashed line represents the fluorescence of RhBITC embedded inside the silica beads, whereas the red solid line represents the fluorescence of RhBITC in a free state. Generally, the aggregation of fluorophores leads to a red-shift of the emission wavelength. In this case, the wavelength is negligibly shifted, implying that RhBITC's mostly exist separately in the silica beads. This is not unexpected since in this work RhBITC is embedded distinctly into silica beads as a coupling agent. The slight difference in the absorption peak positions in Figure 1b would then

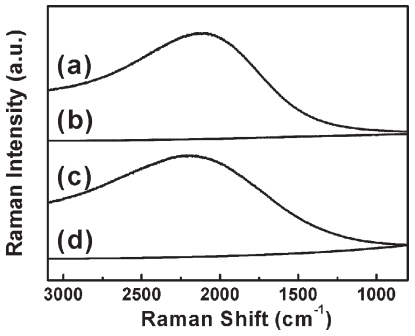

Figure 2. NR spectrum of RhBITC in ethanol taken using (a) 514.5 nm and (b) 632.8 nm radiation as the excitation source, and that of RhBITC-embedded silica beads in ethanol taken using (c) 514.5 nm and (d) 632.8 nm radiation as the excitation source.

be due to the environment (vide supra). Although not shown here, the fluorescence intensity increased proportionally with the concentration of RhBITC.

Spectra a and b in Figure 2 show the normal Raman (NR) spectra of RhBITC in ethanol taken using 514.5 and 632.8 nm radiation as the excitation source, respectively. Both are nearly featureless. The strong background around 2200 cm^{-1} in Figure 2a corresponds to the fluorescence band at 580 nm in Figure 1c. As shown in Figure 2c, the Raman spectrum taken for RhBITC-embedded silica beads using 514.5 nm radiation also exhibits a strong background around 2200 cm^{-1} without any vibrational structure. The Raman spectrum taken using 632.8 nm radiation (Figure 2d) has a quiet background, but it is still difficult to identify any peaks of RhBITC because of the small amount present in the sample.

Modification of Dye-Embedded SiO_2 Beads. As described in the Experimental section, silver was deposited onto the RhBITC-embedded silica beads by soaking them in an ethanolic solution of $AgNO_3$ and butylamine.[31,36] Figure 3a shows the FE-SEM image taken after the deposition of silver onto the beads. The deposition of silver could also be confirmed from the XRD data. As Ag is deposited onto the silica particles, four distinct XRD peaks are clearly observed at 2θ values of 38.1, 44.3, 64.4, and 77.3° in Figure 3b, corresponding to the reflections of the (111), (200), (220), and (311) crystalline planes of cubic Ag, respectively.[37] According to the Debye−Scherrer equation, the size of the Ag nanoparticles formed in a 1:1 mixture of $AgNO_3$ and butylamine was estimated to be ~15 nm. The deposition of aggregated Ag nanoparticles could also be confirmed by the UV/vis spectrum shown in Figure 3c. Compared to the spectrum in Figure 1b, a very broad band appeared, upon the deposition of silver, extending from the near-UV to near-infrared regions. This must be due to a network-like Ag nanoaggregate formed on the silica beads.

Spectra a and b in Figure 4 show the Raman spectra taken using 514.5 and 632.8 nm radiation as the excitation source, respectively, for Ag-coated silica beads embedded with RhBITC. Still no Raman signature of RhBITC is found in either spectra although the presence of RhBITC inside the silica beads can be discerned from the fluorescence background signal around 2200 cm^{-1} in Figure 4a. Most likely this reflects the fact that silver surfaces directly in contact with silica beads are very smooth and do not exhibit measurable SERS activity toward RhBITC contained inside the beads. The background signal in Figure 4a is about one-half as intense as that observed in the NR spectrum in Figure 2c. This suggests that fluorescence quenching took place partly by the deposition of silver onto the silica beads.

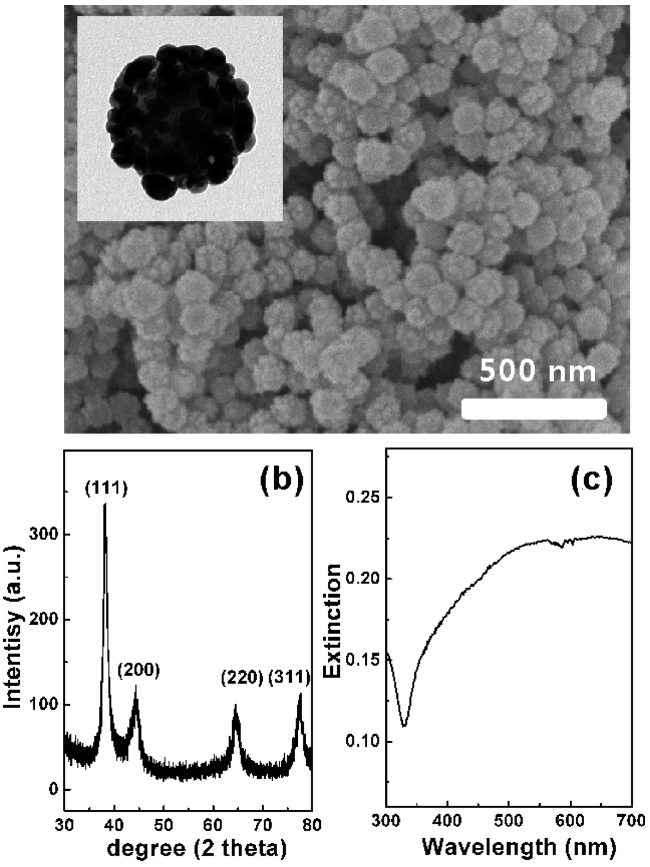

Figure 3. (a) FE-SEM image, (b) XRD pattern, and (c) UV/vis extinction spectrum taken after deposition of silver onto RhBITC-embedded silica beads. The inset in a is an enlarged image of one bead.

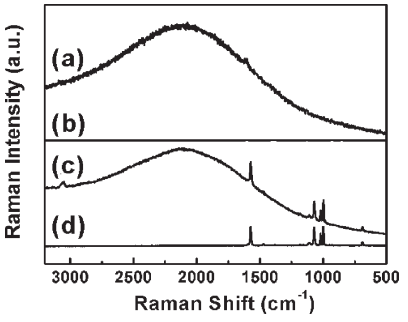

Figure 4. Raman spectrum of Ag-coated, RhBITC-embedded silica beads taken using (a) 514.5 and (b) 632.8 nm radiation as the excitation source and that taken after the adsorption of BT onto Ag-coated, RhBITC-embedded silica beads using (c) 514.5 and (d) 632.8 nm radiation as the excitation source.

The remaining fluorescence signal is, however, strong enough to be detected by a fluorospectrometer (vide infra).

As might be expected from the SEM image in Figure 3a, the silver surfaces coating the outside of the silica beads are highly SERS active. Spectra c and d in Figure 4 show the SERS spectra taken using 514.5 and 632.8 nm radiation as the excitation source, respectively, after the adsorption of BT onto the Ag-coated beads. Although not shown here, the SERS peaks of BT in Figure 4d (normalized with respect to a silicon band at 520 cm^{-1}) are 10 times stronger than the SERS peaks of BT assembled on 2 μm sized μAg powders;

commercially available μAg powders are known to be effective substrates for the IR and Raman spectroscopic characterization of the molecules adsorbed on Ag. Recalling the fact that the surface enhancement factor (EF) of Ag powders is $\sim 1 \times 10^6$, the EF value of the Ag-coated silica beads is as large as $\sim 1 \times 10^7$.

Having confirmed that the Ag-deposited silica beads are highly SERS active substrates, we carried out a silanization reaction to protect the SERS marker molecules assembled on Ag. It is not easy to control silicification if performed directly onto the SERS marker molecules. We demonstrated recently that once the SERS marker molecules are coated with aliphatic polyelectrolytes such as PAH, the base-catalyzed silanization can be readily carried out to form stable silica shells around the polyelectrolyte layers by a biomimetic process.[28] The electrostatic interactions between organic polycations and anionic silica species appear to be one of the main factors controlling silicification. The basic property of the amine moieties in PAH is also supposed to facilitate the silanization reaction. Associated with this reaction, another noteworthy point is that polyelectrolytes can be deposited on any substrates, regardless of their surface charges, via electrostatic and/or van der Waals interactions. We confirmed recently using infrared spectroscopy that the peak intensities of the ν(C═O) and $\nu_{as}(COO^-)$ bands of PAA increase linearly as a function of the LbL deposition cycles of PAA and PAH onto BT-, as well as 4ABT-adsorbed Ag surfaces.[28,38,39] According to the ellipsometric thickness measurement, a three bilayers of PAA and PAH is as thick as ~10 nm.[27] The silanization reaction in this work was thus carried out after three bilayers of PAA and PAH were deposited onto BT- or 4ABT-adsorbed Ag-coated, RhBITC-embedded silica beads.

Figure 5a shows the TEM image taken after the silanization of the BT-adsorbed silica beads. From the TEM image, the silica shell thickness is estimated to be about 20 nm. From the TEM image alone, it is not evident; however, whether the Ag-coated beads are fully covered with silica shells free of any defect. We thus conducted a place exchange reaction to occur on BT on Ag with RhBITC. RhBITC is a very strong Raman scatterer, adsorbing on Ag as likely as BT. When unmodified beads are soaked in the dye, the RhBITC peaks are identified immediately. However, we do not observe any RhBITC peak when silanized beads are subjected to the place exchange reaction with RhBITC for 24 h. As shown in Figure 5b, the observed Raman spectrum is exclusively due to BT. Much the same observation was made using 4ABT-adsorbed silica beads, as can be seen in Figure 5c. This clearly illustrates that the SERS-markers are coated with silica shells without any defect. The exclusive appearance of the Raman peaks due to BT in Figure 5b and 4ABT in Figure 5c is not surprising because aliphatic polyelectrolytes such as PAA and PAH and inorganic materials such as silica are weak Raman scatterers,[40] and the SERS signal must be derived mostly from the adsorbate that is in direct contact with the SERS substrates in accordance with electromagnetic and chemical enhancement mechanisms.[41,42] Hence, if the silica shells are modified with molecular recognition units, the particles can be used as molecular sensors operating via both SERS and fluorescence. To confirm its feasibility, we have conducted additional experiments to differentiate the interaction of h-IgG with anti-h-IgG from that of r-IgG with anti-r-IgG.

Detection of Antigens. The silica-shell-coated particles were first reacted with APTS to have amine functionality and then with GA for the immobilization of anti-h-IgG or anti-r-IgG. These antibody-modified particles can be represented as either RhBITC-SiO_2@Ag/BT@SiO_2-anti-h-IgG or RhBITC-SiO_2@Ag/4ABT@-SiO_2-anti-r-IgG. Separately, we prepared nonfluorescent glass slides grafted in a similar way with anti-h-IgG or anti-r-IgG, and immersed them in a 1×10^{-11} to 1×10^{-4} g mL^{-1} solution of h-IgG or r-IgG

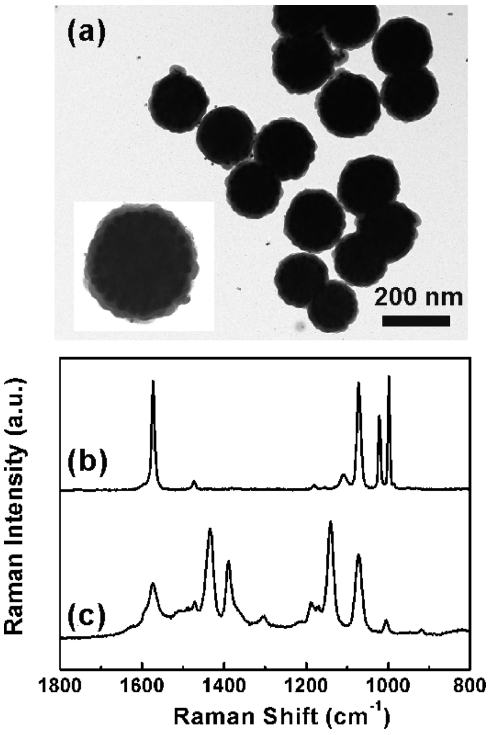

Figure 5. (a) TEM image taken after the silanization of the BT-adsorbed Ag-coated, RhBITC-embedded silica beads. Raman spectra taken after the silanized samples of the (b) BT- and (c) 4ABT-adsorbed Ag-coated, RhBITC-embedded silica beads were soaked in 0.1 mM ethanolic solution of RhBITC for 24 h.

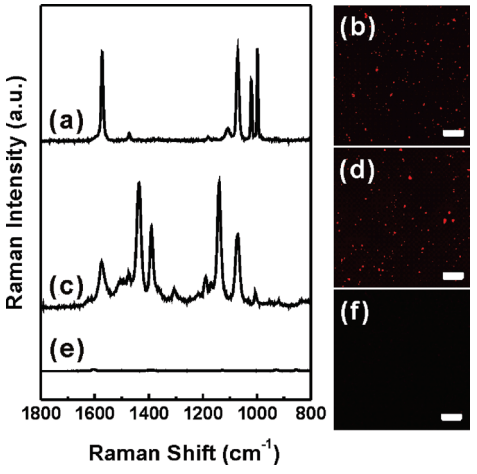

Figure 6. (a, c, e) Raman spectra and (b, d, f) CLSM images obtained after (a, b) anti-h-IgG modified RhBITC-SiO_2@Ag/BT@SiO_2 beads had been allowed to interact via h-IgG with other anti-h-IgG modified layers on glass, (c , d) anti-r-IgG modified RhBITC-SiO_2@Ag/4ABT@SiO_2 beads had been allowed to interact via r-IgG with other anti-r-IgG modified layers on glass, and (e, f) anti-r-IgG modified RhBITC-SiO_2@Ag/4ABT@SiO_2 beads had been allowed to interact via h-IgG with other anti-r-IgG modified layers on glass. The Raman spectra were taken using 632.8 nm radiation as the excitation source. The scale bars in CLSM images represent 20 μm.

for 30 min. Thereafter, these modified glass slides were incubated for 3 h in a solution containing either the RhBITC-SiO_2@Ag/BT@SiO_2-anti-h-IgG or RhBITC-SiO_2@Ag/4ABT@SiO_2-anti-r-IgG. Parts a and b of Figure 6 show, respectively, the Raman

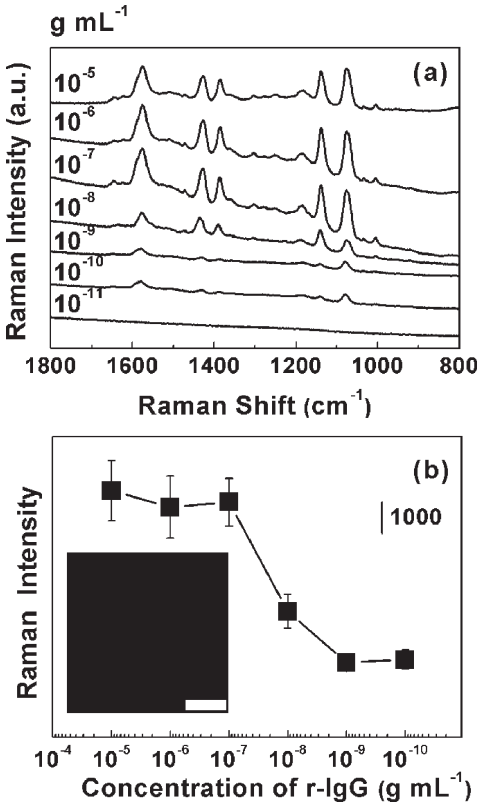

Figure 7. (a) SERS spectra of 4ABT measured after RhBITC-SiO_2@Ag/4ABT@SiO_2-anti-r-IgG beads had been exposed to interact via different amounts of r-IgG with other anti-r-IgG modified glass slide. (b) Normalized SERS intensity of the characteristic band of 4ABT at 1078 cm^{-1} measured as a function of concentrations of r-IgG; the SERS intensities were the average of five different measurements. The inset in b is a CLSM image taken separately during the dose−response experiment with the r-IgG concentration of 1×10^{-10} g mL^{-1}. The scale bar represents 20 μm.

spectrum and CLSM image obtained from the glass slide grafted initially with anti-h-IgG and then soaked in 10^{-4} g mL^{-1} solution of h-IgG; in this work, a confocal microscope was used instead of a conventional (wide-field) fluorescence microscope in order to increase optical resolution and contrast of micrograph. The Raman peaks can be attributed to BT, illustrating that anti-h-IgG-grafted silica beads have interacted, via the mediation of h-IgG, with other anti-h-IgG assembled on a glass slide. Similarly, parts c and d of Figure 6 show, respectively, the Raman spectrum and CLSM image obtained from the glass slide grafted initially with anti-r-IgG and then soaked in 1×10^{-4} g mL^{-1} solution of r-IgG. The Raman peaks can be attributed exclusively to 4ABT, indicating that anti-r-IgG grafted silica beads have bonded, via the mediation of r-IgG, onto a glass slide grafted initially with anti-r-IgG. Parts e and f of Figure 6 represent, respectively, the Raman spectrum and the CLSM image taken after a glass slide grafted initially with anti-r-IgG had been soaked consecutively in a solution containing h-IgG and then in a solution containing anti-r-IgG grafted silica beads. In this case, no Raman peak or CLSM image was identified, suggesting that nonspecific binding was successfully avoided.

We have to mention that the Raman spectral intensities, as well as CLSM signals, decreased with the decrease of r-IgG concentrations, but fairly intense Raman spectra and CLSM images are obtained as long as the r-IgG concentrations are above 1×10^{-10} g mL^{-1}, as shown in Figure 7. To construct a dose−response curve, the anti-r-IgG and r-IgG were chosen as a model system. Briefly, the substrate modified with anti-r-IgG was immersed in a solution containing different amounts of r-IgG, ranging from 1×10^{-5} to 1×10^{-11} g mL^{-1}. The SERS spectral feature is the same as that in Figure 6c. The SERS signals are from 4ABT and their intensities varied with different concentrations of r-IgG. The Raman spectral intensities decreased with the decrease of r-IgG concentrations. We need to admit that accurate quantitative analysis of the concentration of antigen is difficult using this dose−response curve because the Raman intensity does not show a linear relationship along the concentration of r-IgG. However, fairly intense Raman spectra are obtained as long as the r-IgG concentrations are above 1×10^{-10} g mL^{-1}. These observations clearly support our claim that the Ag-coated dye-embedded silica beads can be used as core materials of dual tagging sensors operating via both SERS and fluorescence; signals may be collected either spectroscopically (SERS spectra) or by imaging (as might be required for intracellular studies). In specific terms, the fluorescence signal can be used as a fast readout system of molecular recognition, whereas the SERS signals are used subsequently as the signature of specific molecular interactions.

4. CONCLUSIONS

We have developed a new type of dual-tag sensor, operating via both SERS and fluorescence, for immunoassays. Initially, dye-embedded silica beads were prepared, and then SERS-active Ag was coated thereon via a very simple electroless-plating method. After Raman labels were adsorbed (BT or 4ABT) on Ag, three bilayers of PAA and PAH were deposited onto them by the LBL method, and then enclosed further by a silica shell. After modifying the silica shell consecutively with APTS and GA, either anti-h-IgG or anti-r-IgG was immobilized thereon. Finally, we confirmed, by monitoring the SERS peaks of BT and the CLSM of RhBITC, that anti-h-IgG-grafted particles interact exclusively with h-IgG. Similarly, we confirmed from the SERS peaks of 4ABT, as well as the CLSM of RhBITC, that anti-r-IgG-grafted particles interact solely with r-IgG. These observations clearly illustrate that first, the binding event of the target molecule and then the specific type of antigen can be recognized consecutively by fluorescence and SERS, respectively. We also confirmed that antibody-grafted particles could recognize antigens down to 1×10^{-10} g mL^{-1} solely by the SERS peaks of the Raman markers. The application prospects of these materials are thus expected to be very high, especially in the areas of biological sensing and recognition that rely heavily on optical and spectroscopic properties.

AUTHOR INFORMATION

Corresponding Author

*E-mail: kwankim@snu.ac.kr (K.K.); kshin@ssu.ac.kr (K.S.S.). Tel: +82-2-8806651 (K.K.); +82-2-8200436 (K.S.S.). Fax: +82-2-8891568 (K.K.); +82-2-8244383 (K.S.S.).

ACKNOWLEDGMENT

This work was supported by National Research Foundation of Korea Grant funded by the Korean Government (Grant 2010-0001637, M10703001067-08M0300-06711-Nano2007-02943, KRF-2008-313-C00390, and 2009-0072467).

REFERENCES

(1) Ma, Z.; Sui, S.-F. *Angew. Chem., Int. Ed.* **2002,** *41*, 2176–2179.
(2) Xu, S.; Ji, X.; Xu, W.; Zhao, B.; Dou, X.; Bai, Y.; Ozaki, Y. *J. Biomed. Opt.* **2005,** *10*, 0311121−1–12.

(3) Płaza, G.; Ulfig, K.; Tien, A. J. *Pol. J. Environ. Stud.* **2000,** *9,* 231–236.
(4) Baker, G. A.; Moore, D. S. *Anal. Bioanal. Chem.* **2005,** *382,* 1751–1770.
(5) Gutcho, S.; Mansbach, L. *Clin. Chem.* **1977,** *23,* 1609–1614.
(6) Vuori, J.; Rasi, S.; Takala, T.; Väänänen, K. *Clin. Chem.* **1991,** *37,* 2087–2092.
(7) Xu, Y. -Y.; Pettersson, K.; Blomeberg, K.; Hemmila, I.; Mikola, K.; Lovgren., T. *Clin. Chem.* **1992,** *38,* 2038–2043.
(8) Brown, C. R.; Higgins, K. W.; Frazer, K.; Schoelz, L. K.; Dyminski, J. W.; Marinkovich, V. A.; Miller, S. P.; Burd, J. F. *Clin. Chem.* **1985,** *31,* 1500–1505.
(9) Hayes, F. J.; Halsall, H. B.; Heineman, W. R. *Anal. Chem.* **1994,** *66,* 1860–1865.
(10) Butler, J. E. *J. Immunoassay Immunochem.* **2000,** *21,* 165–209.
(11) Dou, X.; Takama, T.; Yamaguchi, Y.; Yamamoto, H.; Ozaki, Y. *Anal. Chem.* **1997,** *69,* 1492–1495.
(12) Ni, J.; Lipert, R. J.; Dawson, G. B.; Porter, M. D. *Anal. Chem.* **1999,** *71,* 4903–4908.
(13) Rohr, T. E.; Cotton, T.; Fan, N.; Tarcha, P. J. *Anal. Biochem.* **1989,** *182,* 388–398.
(14) Han, X. X.; Cai, L. J.; Guo, J.; Wang, C. X.; Ruan, W. D.; Han, W. Y.; Xu, W. Q.; Zhao., B.; Ozaki., Y. *Anal. Chem.* **2008,** *80,* 3020–3024.
(15) Driskell, J. D.; Uhlenkamp, J. M.; Lipert, R. J.; Porter, M. D. *Anal. Chem.* **2007,** *79,* 4141–4148.
(16) Xu, S.; Ji, X.; Xu, W.; Li, X.; Wang, L.; Bai, Y.; Zhao, B.; Ozaki., Y. *Analyst* **2004,** *129,* 63–68.
(17) Gong, J. L.; Liang., Y.; Huang., Y.; Chen, J. W.; Jiang, J. H.; Shen, G. L.; Yu, R. Q. *Biosens. Bioelectron.* **2007,** *22,* 1501–1507.
(18) Kneipp, K.; Wang, Y.; Kneipp, H.; Perelman, L. T.; Itzkan, I.; Dasari, R. R.; Feld, M. S. *Phys. Rev. Lett.* **1997,** *78,* 1667–1670.
(19) Nie, S.; Emory, S. R. *Science* **1997,** *275,* 1102–1106.
(20) Xu, H.; Bjerneld, E. J.; Käll, M.; Börjesson, L. *Phys. Rev. Lett.* **1999,** *83,* 4357–4360.
(21) Futamate, M.; Maruyama, Y.; Ishikawa, M. *Vib. Spectrosc.* **2002,** *30,* 17–23.
(22) Lyon, L. A.; Keating, C. D.; Fox, A. P.; Baker, B. E.; He, L.; Nicewarner, S. R.; Mulvaney, S. P.; Natan, M. J. *Anal. Chem.* **1998,** *70,* 341R–361R.
(23) Yu, K. N.; Lee, S.-M.; Han, J. Y.; Park, H.; Woo, M.-A.; Noh, M. S.; Hwang, S.-K.; Kwon, J.-T.; Jin, H.; Kim, Y.-K.; Hergenrother, P. J.; Jeong, D. H.; Lee, Y.-S.; Cho, M.-H. *Bioconjugate Chem.* **2007,** *18,* 1155–1162.
(24) Woo, M.-A.; Lee, S.-M.; Kim, G.; Baek, J. H.; Noh, M. S.; Kim, J. E.; Park, S. J.; Minai-Tehrani, A.; Park, S.-C.; Seo, Y. T.; Kim, Y.-K.; Lee, Y.-S.; Jeong, D. H.; Cho, M.-H. *Anal. Chem.* **2009,** *81,* 1008–1015.
(25) Pallaoro, A.; Braun, G. B.; Reich, N. O.; Moskovits, M. *Small* **2010,** *6,* 618–622.
(26) Kim, K.; Lee, Y. M.; Lee, H. B.; Shin, K. S. *ACS Appl. Mater. Interfaces* **2009,** *1,* 2174–2180.
(27) Kim, K.; Lee, Y. M.; Lee, H. B.; Shin, K. S. *Biosens. Bioelectron.* **2009,** *24,* 3615–3621.
(28) Kim, K.; Lee, H. B.; Shin, K. S. *Langmuir* **2008,** *24,* 5893–5898.
(29) Bagwe, R. P.; Yang, C.; Hilliare, L. R.; Tan, W. *Langmuir* **2004,** *20,* 8336–8342.
(30) Santra, S.; Zhang, P.; Wang, K.; Tapec, R.; Tan, W. *Anal. Chem.* **2001,** *73,* 4988–4993.
(31) Kim, K.; Lee, H. B.; Lee, Y. M.; Shin, K. S. *Biosens. Bioelectron.* **2009,** *24,* 1864–1869.
(32) Sato, H.; Kidaka, T.; Hori, M. *Appl. Biochem. Biotechnol.* **1987,** *15,* 145–158.
(33) Tuong, S. D.; Lee, H.; Kim, H. *Macromol. Res.* **2008,** *16,* 373–378.
(34) Wang, C.; Chen, Y.; Wang, T.; Ma, Z.; Su, Z. *Adv. Funct. Mater.* **2008,** *18,* 355–361.
(35) Socrates, G. *Infrared Characteristic Group Frequencies: Tables and Charts*; John Wiley & Sons: Chichester, U.K., 1994.
(36) Kim, K.; Kim, H. S.; Park, H. K. *Langmuir* **2006,** *22,* 8083–8088.
(37) He, R.; Qian, X.; Yin, J.; Zhu, Z. *J. Mater. Chem.* **2002,** *12,* 3783–3786.
(38) Kim, K.; Lee, H. S.; Yu, H. D.; Park, H. K.; Kim, N. H. *Colloid Surf., A* **2008,** *316,* 1–7.
(39) Kim, K.; Park, H. K.; Kim, N. H. *Langmuir* **2006,** *22,* 3421–3427.
(40) Mulvaney, S. P.; Musick, M. D.; Keating, C. D.; Natan, M. J. *Langmuir* **2003,** *19,* 4784–4790.
(41) Chang, R. K.; Furtak, T. E., *Surface Enhanced Raman Scattering*; Plenum Press: New York. 1982.
(42) Moskovits, M. *Rev. Mod. Phys.* **1985,** *57,* 783–826.